Dentomaxillofacial Radiology (2014) 43, 20130332

http://birpublications.org

RESEARCH ARTICLE

Accuracy of CBCT images in the assessment of buccal marginal alveolar peri-implant defects: effect of field of view

[1,2]K Kamburoğlu, [3,4]S Murat, [5]C Kılıç, [6]S Yüksel, [7]H Avsever, [2]A Farman and [2]W C Scarfe

[1]Department of Dentomaxillofacial Radiology, Faculty of Dentistry, Ankara University, Ankara, Turkey; [2]Radiology and Imaging Sciences, Department of Surgical Hospital Dentistry, University of Louisville School of Dentistry, KY, USA; [3]Department of Prosthetic Dentistry, Faculty of Dentistry, Istanbul Aydin University, Istanbul, Turkey; [4]Department of Maxillofacial Prosthodontics, James Graham Brown Cancer Center, University of Louisville, KY, USA; [5]Department of Anatomy, Gülhane Military Medical Academy, Ankara, Turkey; [6]Department of Biostatistics, Faculty of Medicine, Yıldırım Beyazıt University, Ankara, Turkey; [7]Department of Dentomaxillofacial Radiology, Dental Science Center, Gülhane Military Medical Academy, Ankara, Turkey

Objectives: To investigate the reliability and accuracy of cone beam CT (CBCT) images obtained at different fields of view in detecting and quantifying simulated buccal marginal alveolar peri-implant defects.

Methods: Simulated buccal defects were prepared in 69 implants inserted into cadaver mandibles. CBCT images at three different fields of view were acquired: 40×40, 60×60 and 100×100 mm. The presence or absence of defects was assessed on three sets of images using a five-point scale by three observers. Observers also measured the depth, width and volume of defects on CBCT images, which were compared with physical measurements. The kappa value was calculated to assess intra- and interobserver agreement. Six-way repeated analysis of variance was used to evaluate treatment effects on the diagnosis. Pairwise comparisons of median true-positive and true-negative rates were calculated by the χ^2 test. Pearson's correlation coefficient was used to determine the relationship between measurements. Significance level was set as $p < 0.05$.

Results: All observers had excellent intra-observer agreement. Defect status ($p < 0.001$) and defect size ($p < 0.001$) factors were statistically significant. Pairwise interactions were found between defect status and defect size ($p = 0.001$). No differences between median true-positive or true-negative values were found between CBCT field of views ($p > 0.05$). Significant correlations were found between physical and CBCT measurements ($p < 0.001$).

Conclusions: All CBCT images performed similarly for the detection of simulated buccal marginal alveolar peri-implant defects. Depth, width and volume measurements of the defects from various CBCT images correlated highly with physical measurements.

Dentomaxillofacial Radiology (2014) **43**, 20130332. doi: 10.1259/dmfr.20130332

Cite this article as: Kamburoğlu K, Murat S, Kılıç C, Yüksel S, Avsever H, Farman A, et al. Accuracy of CBCT images in the assessment of buccal marginal alveolar peri-implant defects: effect of field of view. *Dentomaxillofac Radiol* 2014; **43**: 20130332.

Keywords: peri-implant defects; CBCT; radiography; FOV; voxel size

Introduction

Success of dental implant treatment mainly depends on the sustainable long-term health of soft and hard peri-implant tissues. Assessment of mobility, pain, infection, inflammation and marginal alveolar bone loss are all considered as useful implant success criteria.[1,2] Specific attention has been directed towards post-operative radiographic assessment of marginal alveolar bone loss around implants by serial intraoral radiographs.[3–7] Vertical marginal bone loss at the peri-implant surfaces should not exceed 1–2 mm during the first year of

Correspondence to: Dr Kıvanç Kamburoğlu. E-mail: kamburogluk@dentistry.ankara.edu.tr
First two authors were supported by The Scientific and Technological Research Council of Turkey, Scientific Fellowships and Grant Programmes Department (TUBITAK-BIDEB Programme No. 2219 and No. 2214).
Received 7 September 2013; revised 10 March 2014; accepted 18 March 2014

function and 0.2 mm thereafter.[6] A decrease in bone level vertical height due to perioperative surgical trauma and\or occlusal overloading can be associated with a loss in the implant's bony anchorage.[7]

Post-insertion radiographic assessment of implant fixtures is usually performed using intraoral periapical projections.[7] These images demonstrate the mesial and distal aspects of the alveolar bone/fixture interface and marginal alveolar bone tangential to the X-ray beam. However, initial post-insertion bone loss occurs mostly on the facial or buccal aspect of the dental implant, since bone is thin on these sides of the implants.[8] Periapical images not only are limited in detecting initial peri-implant bone loss but also underestimate the actual size of the defect as well as being unable to provide volumetric information about the status of such defects, which is important in monitoring progression or resolution after therapy.[7,8] Moreover, inter- and intra-observer variability in the interpretation of two-dimensional images is high.[9–14] Given these limitations, there is a clinical need for objective and quantitative methods for detecting marginal alveolar peri-implant status.

Maxillofacial cone beam CT (CBCT) is a volumetric acquisition technique providing accurate and reliable submillimetre resolution images in all spatial dimensions, which shows promise in the detection of peri-implant defects.[15–18] However, unlike intraoral radiography, if metallic objects such as amalgam or titanium implants are present in the CBCT scan, two artefacts can be produced degrading image quality. Streak artefacts due to the presence of scatter radiation as linear hyperdensities radiating from the metallic object might extend to the entire width of the field, affecting even the visualization of areas on the opposite side of the jaw.[15,19] Beam hardening artefacts appear as dark voids adjacent to high-density structures, such as titanium implants, and are due to the differential absorption of low-energy X-ray photons by high-density materials.[19,20] The severity of these artefacts produced by dental implants on image quality has been reported to be greater for CBCT than for multislice CT,[21] to be CBCT unit dependent,[22] to influence the reliability of linear measurements of adjacent marginal bone[23] and to vary depending on the implant surface, with increasing Gray values occurring on buccal and lingual aspects.[24]

Field of view (FOV) is the term used to refer to the scan volume of a particular CBCT unit. FOV is determined by detector size and shape, beam projection geometry and beam collimation, which limits radiation exposure to a particular region of interest. A "voxel" describes the smallest distinguishable box-shaped part of a three-dimensional image. In CBCT imaging, voxels are isotropic, and images can be constructed in any plane with high fidelity. The availability of different FOVs makes it possible to select the most appropriate FOV for a specific application. Because larger FOVs result in higher effective radiation doses, as a rule, smaller FOVs are recommended for imaging a quadrant or single tooth. Selection of FOV and voxel size can be detrimental in the diagnosis of peri-implant defects. It is possible to obtain smaller voxel sizes with smaller FOVs. CBCT can improve the spatial resolution of high-contrast structures in any chosen viewing plane. This superior spatial resolution, that is, the ability to discriminate objects of different attenuation separated by very small distances, is one of the most attractive qualities of CBCT imaging.[15,25] However, no general protocol is currently defined for CBCT examination of specific diagnostic tasks in dentistry taking into consideration voxel size variation.[26]

Using *ex vivo* mandibular bone, the purpose of this study is two-fold: (1) to compare the reliability and detection rates of simulated buccal peri-implant defects by CBCT images obtained with various FOVs; and (2) to compare the accuracy and reproducibility of linear (depth and width) and volumetric measurements of simulated buccal peri-implant defects by CBCT images to actual physical measurements of the simulated defects.

Methods and Materials

Sample and implant placement

Approval of the use of cadaver mandibles ($n = 5$) was obtained through the Department of Anatomy, Gülhane Military Medical Academy, Ankara, Turkey (Local Ethical Committee Review No. 1491-304-12/1539-605). A total of 69 ($n = 69$) dental implants were used from two manufacturers; 31 ($n = 31$) were MIS (MIS Implants Technologies Ltd., Shlomi, Israel) (diameter range, 3.75–4.20 mm; length range, 10–13 mm) and 38 were ($n = 38$) Oxy Implants (Biomec SRL, Colico, Italy) (diameter range, 3.75–4.25 mm; length range, 9–13 mm) with aggressive thread design. Implants were randomly inserted into pre-molar and molar regions of denuded cadaver mandibles by an experienced operator. Implants were placed close to the buccal aspect of the mandible to facilitate creation of artificial defects in the buccal cortical marginal alveolar bone. Mandibles were then separated by a bone saw into equal smaller sections, each one comprising two or three implants, and 1.5 cm of wax was applied to the mandibular sections as a soft tissue equivalent material. Each section was flattened, levelled and placed on a putty impression material for stabilization (Figure 1a).

Simulated defect creation

After implant placement, mechanical cavities of various sizes and dimensions simulating localized peri-implant marginal defects were prepared on the buccal aspect of the marginal alveolar cortical bone using round and cylindrical dental burs to their full depth. Dimensional measurements of the maximum width and depth (from the top of the fixture to the bottom of the bone loss margin) of the defects were performed twice by an anatomist using an electronic digital calliper (Allendale Electronics Ltd., Hertfordshire, UK) with fine-pointed jaws and measuring range of 0–200 mm (0–8.0 inch) and

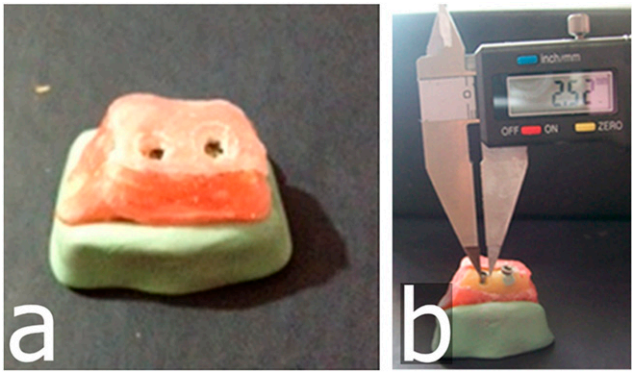

Figure 1 Representative mandibular section with two implants. (a) A mandibular section with two implants covered with wax material and placed on a putty impression; (b) an implant with prepared buccal marginal alveolar peri-implant defect showing measured width using a digital calliper.

a resolution of 0.01 mm (0.0005 inch). The average of both measurements was considered as the reference standard (Figures 1b, 2a). Defects were classified according to their depths and widths as small [defects with depth and/or width between 1 and 3 mm (<3 mm)], medium (defects with depth and/or width between 3 and 5 mm) or large (defects with depth and/or width >5 mm). There were 29 small, 24 medium and 16 large defects. In addition, a non-deformable light flow silicon impression material (Variotime®; Heraeus-Kulzer, Hanau, Germany) was injected into 21 randomly selected well-defined defects (Figure 2b), and volumes of the impression models were measured by a "water displacement technique". This technique uses the following principle: lost volume of the water in the cylinder − initial volume of the water in the cylinder = defect volume. Volumetric measurements of the impression models were made using a SCALTEC SBC 21 balance (Denver Instrument, Bohemia, NY) by an external independent researcher (physiologist). The average volume was considered the reference standard. All physical measurements were then compared with CBCT image measurements.

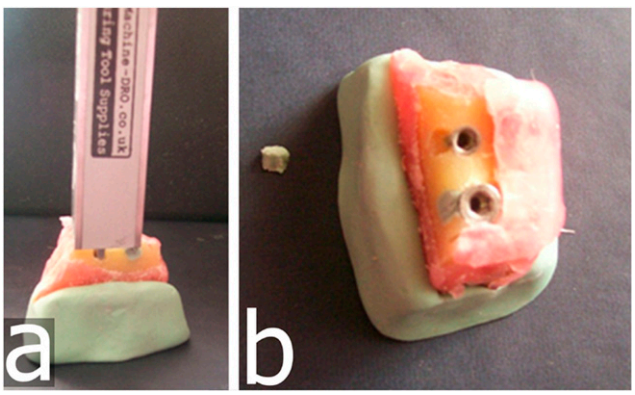

Figure 2 Representative implant with prepared buccal marginal alveolar peri-implant defect showing (a) measured depth by a digital calliper and (b) impression of corresponding buccal marginal alveolar peri-implant defects.

Imaging

Images of the implants inserted in the mandibles were obtained using a complementary metal-oxide semiconductor flat panel detector, variable FOV CBCT unit (3D Accuitomo 170; J Morita Mfg. Corp., Kyoto, Japan) operating at 90 kVp, 5.0 mA and an exposure time of 17.5 s to image each specimen before and after defect preparation at three different FOVs and voxel sizes [nominal cubic millimetre resolution (mm^3)]: (1) 40×40 mm FOV, 0.080 mm^3 (FOV_{40}); (2) 60×60 mm FOV, 0.125 mm^3 (FOV_{60}); and (3) 100×100 mm FOV, 0.250 mm^3 (FOV_{100}).

Data collection

A total of three image sets were obtained: (1) FOV_{40}; (2) FOV_{60}; and (3) FOV_{100}. Images were viewed by three experienced observers in a dimly lit room on a 15.6-inch laptop monitor (Qosmio® F75 5-3D350; Toshiba, Tokyo, Japan) at a screen resolution of 1920×1080 pixels and 32-bit colour depth. Image sets were viewed at 1-week intervals, and repetitions were performed 1 month after the initial viewings. For CBCT evaluations, proprietary manufacturer software (i-Dixel 2.0/One Data Viewer/One Volume Viewer; J Morita Mfg. Corp.) was used.

All implants were randomly evaluated for the presence or absence of buccal defects, and observers were instructed to use a 5-point scale: 1 = defect definitely present; 2 = defect probably present; 3 = uncertain or unable to tell; 4 = defect probably not present; and 5 = defect definitely not present. When a defect was detected by an evaluator on CBCT observations, he/she was asked to use the i-Dixel to provide quantitative linear measurements. Maximum width and depth measurements of defects for CBCT images were measured twice, and the average was calculated (Figure 3). Only measurements obtained from detected true-positive defects were included in the analysis. CBCT measurements were then compared with calliper measurements.

For volumetric measurements, axial CBCT scans taken at each acquisition parameter of 21 well-defined defects were exported as digital imaging and communications in medicine files and then imported into a volumetric rendering software capable of measuring vector-based segmentation technology (3D-DOCTOR™; Able Software Corp., Lexington, MA). This software allows defect segmentation on consecutive axial slices, enabling defect visualization at each level apico-coronally. This ensured detailed slice-by-slice segmentation of the defect borders manually using a mouse with colour delineation. Automated calculation of the total volume from the areas outlined on each slice of known thickness (0.4 mm) was performed by the software. This was performed twice by two of the three observers, and the average was compared with the physical volume calculated from the impression material (Figure 4).

Statistical analyses

As reference standard categories were dependent, kappa values were calculated to provide an index of intra- and

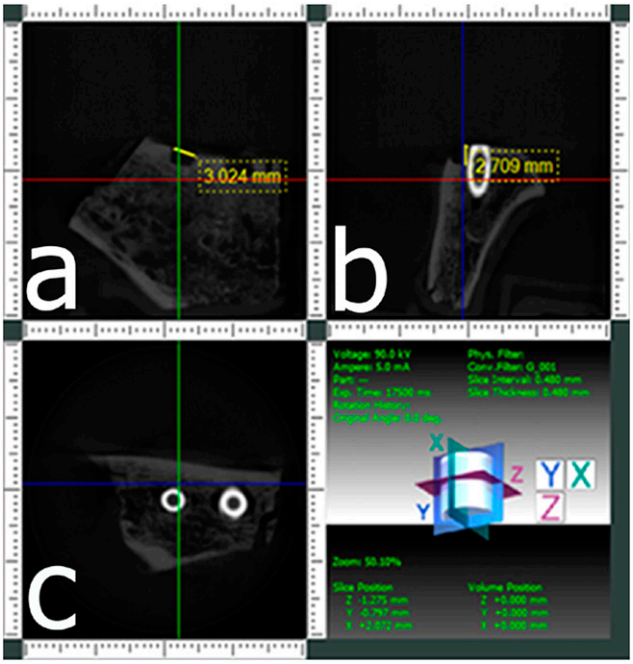

Figure 3 Cone beam CT images from a scan obtained at a 40 × 40 mm field of view of an implant with a buccal marginal alveolar peri-implant defect shown in Figures 1, 2. (a) A coronal section providing the width of the defect, (b) a cross-sectional section providing the depth of the defect and (c) an axial section.

interobserver agreements for each dichotomous situation (defect present *vs* no defect present). Six-way repeated analysis of variance (ANOVA) was used to evaluate the effects of defect status, observer, reading, FOV, implant brand and defect size on the diagnosis with pairwise comparisons. Defect status, observer, reading and FOV were measured as a within-subject effect, whereas implant brand and defect size were measured as a between-subject effect in the model. Only statistically significant effects were included in the ANOVA table. Bonferroni adjustment was used for pairwise comparisons. True-positive (TP) and true-negative (TN) rates were calculated as an index of accuracy. For TP rate calculations, categories one and two and for TN rate calculations, categories four and five were collapsed. Pairwise comparisons of TP and TN rate values were derived from each observer and each reading using the χ^2 test statistics. The Type-I error rate was set at an *a priori* value $\alpha = 0.05$. The Pearson's correlation coefficient was used to display the relationship between actual measurements and depth, width and volume measurements for each observer.

Results

Excellent intra-observer agreements were found for all observers and image sets (Table 1). In general, good and excellent interobserver agreement values were obtained. Table 2 shows the interobserver agreement values according to defect status. Effects of defect status, observer, reading, FOV, implant brand and defect size by using six-way repeated ANOVA are shown in Table 3. Defect status ($p < 0.001$) and defect size ($p < 0.001$) factors were statistically significant. Pairwise interactions were found between defect status and defect size ($p = 0.001$) and defect status, reading and defect size ($p = 0.017$). The defect size alone and pairwise comparison of small and medium defects ($p = 0.021$) and small and large defects ($p < 0.001$) provided statistical differences for the defect present status. The comparison of TP and TN values of various FOVs for each observer and their reading according to size and crosswise comparison between FOVs are given in Table 4. TP values ranged from 0.449 to 0.594, and TN values ranged from 0.855 to 0.957 for overall size and for CBCT images obtained with different FOVs. No differences between overall median TP or TN values were found between CBCT FOVs ($p > 0.05$). Also, for small, medium and large defects, there were no differences with respect to TP and TN values between different CBCT FOVs ($p > 0.05$). Table 5 shows the comparison of actual mean depth, width and volume dimensions with CBCT measurements. The Pearson's correlation coefficient was high, and actual defect size correlated highly with depth

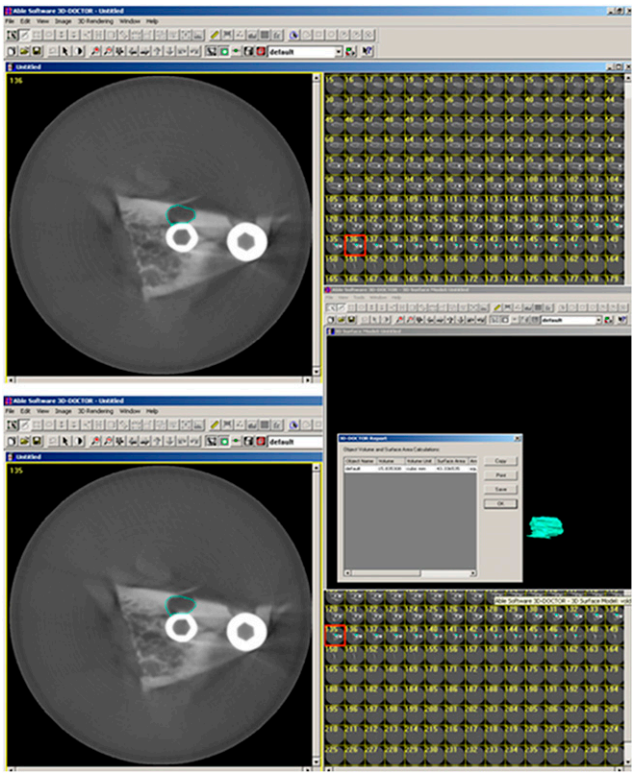

Figure 4 Representative images from 3D-DOCTOR™ analysis software (Able Software Corp., Lexington, MA) illustrating the segmentation process for volume quantification. Each axial slice of the region containing the defect was delineated by a border using the mouse cursor.

Table 1 Intra-observer agreement calculated for each observer by image type according to defect status

	Defect present status			*No defect status*		
	First observer	*Second observer*	*Third observer*	*First observer*	*Second observer*	*Third observer*
Field of view	*Weighted kappa; SE*	*Weighted kappa; SE*	*Weighted kappa; SE*	*Weighted kappa; SE*	*Weighted kappa; SE*	*Weighted kappa; SE*
CBCT (FOV_{40})	0.941; 0.097	0.903; 0.092	0.988; 0.089	0.911; 0.090	0.878; 0.075	0.881; 0.078
CBCT (FOV_{60})	0.904; 0.090	0.879; 0.093	0.982; 0.088	0.983; 0.098	0.841; 0.080	0.908; 0.091
CBCT (FOV_{100})	0.910; 0.095	0.938; 0.090	0.963; 0.090	0.921; 0.089	0.749; 0.065	0.913; 0.092

CBCT, cone beam CT; FOV_{40}, 40 × 40 mm field of view; FOV_{60}, 60 × 60 mm field of view; FOV_{100}, 100 × 100 mm field of view; SE, standard error.

(range, 0.931 and 0.970), width (range, 0.860 and 0.956) and volume (range, 0.913 and 0.977) measurements.

Discussion

The choice of an accurate and reliable imaging modality in the assessment of peri-implant marginal alveolar bone status is clinically important in terms of post-operative monitoring of stability and selection of re-medial treatment. Accurate determination of marginal alveolar defect size and volume might also assist in the selection of appropriate surgical correction procedures including grafting.

In this study, for overall and varying defect sizes, observers using CBCT images taken at three acquisition parameters using different FOVs and resolutions performed similarly in the detection of simulated buccal marginal peri-implant defects with no distinction between the type of CBCT acquisition mode. However, it should be noted that higher median TP values were found for FOV_{40} and FOV_{60} than for FOV_{100} without statistical significance. Detection ability improved with increasing defect size for CBCT images, with small defects being the most difficult to read. We found higher TN than TP values, suggesting better visualization of disease-free implants when compared with diseased implants by observers. In addition, implant type had no effect on observer performance in this research. We could obtain two different implant brands from two different companies. Further studies should be conducted to compare different implant brands in assessing defect visibility around implants. A recent study[19] found that there was no difference in the detection of simulated buccal peri-implant defects among CBCT images obtained with and without the artefact reduction modes of the Planmeca ProMax® 3D Max CBCT unit (Planmeca Oy, Helsinki, Finland). In this study, we did not use any artefact reduction filter as the CBCT unit chosen for this study does not offer different artefact reduction modes.

Depth, width and volumetric measurements of the defect obtained by different CBCT FOVs were accurate and correlated highly with actual dimensions and among observers. Volumetric measurements also showed high correlation with the physical measurements that were considered as the gold standard. We speculated that beam hardening and scatter artefacts from titanium implants would limit the utility of CBCT for buccal marginal alveolar defect detection; however, we found relatively good detection rates for CBCT images, specifically for large and medium defects. This finding could be attributable to our experimental setup in that we imaged only small mandibular sections instead of a full head, the absence of motion artefacts, differential image quality of the CBCT system used and/or the use of experienced clinicians as observers.

Our results differ from those of Schliephake et al,[8] who investigated the ability of different analysis of images from periapical radiography and CT in measuring the marginal peri-implant bone levels at implants with buccal bone defects. They found that both techniques underestimated actual bone loss. In addition, they reported poor correlation of buccal bone measurements with actual bone height and concluded that they are not suitable to provide reliable information on the peri-implant bone level on this surface. Schliephake et al[8] used a CT device with much lower spatial resolution than that of this study (0.6 mm reconstruction increment). This dimension corresponds to the thickness of a thread flank of the implants used and therefore has inherent limitations in imaging the implant/bone interface properly.

A study by Mengel et al[16] compared the accuracy of intraoral radiography, panoramic radiography, medical CT (Prospeed® SX Power; GE Medical Systems, Solingen, Germany) and the same CBCT as used in this present study (3D Accuitomo) to measure the simulated peri-implant defects created similar to the technique used in our study. Their results are in concordance with ours in that they found a mean deviation of 0.17–0.11 mm for the CBCT and 0.18–0.12 mm for the CT scans. Similarly, Corpas Ldos et al[17] compared radiographic and histological findings and found significant correlations (R range, 0.61–0.7) between bone defect depth on intraoral radiography and on CBCT images, leading the authors to suggest that measurements from both radiographic modalities are accurate and reliable for post-operative implant assessment. We found higher mean deviation from the defect status for depth than that for width measurements. This may be owing to the difficulty in determining the exact location of

Table 2 Interobserver agreement values according to defect status

	First readings for defect present status			*Second readings for defect present status*			*First readings for no defect status*			*Second readings for no defect status*		
	First observer–second observer	*First observer–third observer*	*Second observer–third observer*	*First observer–second observer*	*First observer–third observer*	*Second observer–third observer*	*First observer–second observer*	*First observer–third observer*	*Second observer–third observer*	*First observer–second observer*	*First observer–third observer*	*Second observer–third observer*
	Weighted kappa; SE	*Weighted kappa; SE*	*Weighted kappa; SE*	*Weighted kappa; SE*	*Weighted kappa; SE*	*Weighted kappa; SE*	*Weighted kappa; SE*	*Weighted kappa; SE*	*Weighted kappa; SE*	*Weighted kappa; SE*	*Weighted kappa; SE*	*Weighted kappa; SE*
CBCT (FOV_{40})	0.921; 0.098	0.942; 0.097	0.897; 0.081	0.940; 0.098	0.914; 0.091	0.900; 0.089	0.742; 0.087	0.670; 0.086	0.828; 0.078	0.653; 0.072	0.600; 0.065	0.519; 0.071
CBCT (FOV_0)	0.917; 0.096	0.935; 0.091	0.897; 0.076	0.912; 0.092	0.895; 0.085	0.872; 0.086	0.729; 0.083	0.581; 0.074	0.790; 0.081	0.568; 0.070	0.645; 0.072	0.646; 0.078
CBCT (FOV_{100})	0.952; 0.086	0.931; 0.087	0.922; 0.098	0.906; 0.092	0.881; 0.085	0.876; 0.086	0.800; 0.086	0.732; 0.085	0.768; 0.082	0.594; 0.072	0.495; 0.061	0.411; 0.060

CBCT, cone beam CT; FOV_{40}, 40×40 mm field of view; FOV_{60}, 60×60 mm field of view; FOV_{100}, 100×100 mm field of view; SE, standard error.

Table 3 Effects of defect status, observer, reading, field of view, implant brand and defect size by using six-way repeated analysis of variance

Source			df	F	p-*value*
Defect status			1	73.875	<0.001
Defect size			2	9.405	<0.001
Pairwise comparisons	Small	Medium			0.021
	Small	Large			<0.001
Defect status × defect size			2	8.014	0.001
Pairwise comparisons					
Defect present	Small	Medium			0.012
	Small	Large			<0.001
Defect status × reading × defect size			2	4.325	0.017
Defect present					
Reading 1	Small	Medium			0.007
	Small	Large			<0.001
Reading 2	Small	Medium			0.023
	Small	Large			<0.001

Only statistically significant effects were included.
df, degrees of freedom

reference points for depth measurements when using CBCT software. Cavities prepared with burs are normally shaped and well defined, and this could have increased observers' detection ability in this study. We did not use panoramic radiography because of the inability to locate the mandibular sections in the focal trough.

A similar study by Sirin et al[18] compared the detection of peri-implant crestal bone defects of increasing diameter using periapical radiography, direct digital radiography, panoramic radiography, CBCT and multislice CT. They found similar intra- and interobserver agreement levels and lower detection rates for multislice CT with comparable rates for all other modalities. Unlike the Sirin et al[18] study, we did not assess decision-making speed or image quality of different radiographic modalities as these variables are relatively subjective and observer dependent. In addition, observers in the above mentioned study[18] assessed circumferential defects, whereas we investigated buccal defects only, which are clinically more difficult to detect.

Razavi et al[27] compared the ability of two different CBCT systems [i-CAT Next Generation (NG); Imaging Sciences International, Hatfield, PA and Accuitomo 3D 60 FPDs; J Morita Mfg. Corp.] in determining the cortical bone thickness adjacent to dental implants and found the system with the lower resolution (i-CAT) to be less accurate. Considering the reduced visibility of subtle bone structures when CBCT units using $>0.3\,mm^3$ are used, we preferred an acquisition parameter less than this apparent threshold. The validity of this approach for subsequent clinical protocols is substantiated in that our CBCT linear and volumetric measurements correlated highly with the direct physical measurements.

The validity and accuracy of the water displacement technique and image segmentation methodology that we used to measure volume from direct impressions and on images, respectively, have been previously

Table 4 Comparison of true-positive and true-negative values of different cone beam CT field of views (FOVs) for each observer and their reading for small, medium, large and overall sizes

Observer and reading	*Accuracy rates*	*Small*			*Medium*			*Large*			*Overall*		
		FOV_{40}	FOV_{60}	FOV_{100}	FOV_{40}	FOV_{60}	FOV_{100}	FOV_{40}	FOV_{60}	FOV_{100}	FOV_{40}	FOV_{60}	FOV_{100}
First observer–first reading	TPR	0.594	0.565	0.478	0.667	0.667	0.583	0.875	0.875	0.750	0.594	0.565	0.478
	TNR	0.913	0.855	0.899	0.958	0.833	0.875	0.813	0.813	0.875	0.913	0.855	0.899
First observer–second reading	TPR	0.594	0.580	0.536	0.667	0.667	0.667	0.813	0.813	0.750	0.594	0.580	0.536
	TNR	0.942	0.855	0.913	0.958	0.833	0.875	0.875	0.813	0.875	0.942	0.855	0.913
Second observer–first reading	TPR	0.565	0.551	0.464	0.625	0.625	0.542	0.938	0.750	0.713	0.565	0.551	0.464
	TNR	0.913	0.928	0.870	0.917	0.917	0.833	0.938	0.938	0.938	0.913	0.928	0.870
Second observer–second reading	TPR	0.565	0.551	0.493	0.667	0.625	0.583	0.813	0.875	0.750	0.565	0.551	0.493
	TNR	0.942	0.942	0.957	0.958	0.875	0.917	0.938	0.938	0.938	0.942	0.942	0.957
Third observer–first reading	TPR	0.565	0.507	0.449	0.625	0.625	0.542	0.875	0.875	0.813	0.565	0.507	0.449
	TNR	0.913	0.913	0.899	0.917	0.917	0.917	0.938	0.938	0.875	0.913	0.913	0.899
Third observer–second reading	TPR	0.565	0.507	0.464	0.625	0.625	0.583	0.875	0.875	0.813	0.565	0.507	0.464
	TNR	0.913	0.913	0.913	0.917	0.917	0.958	0.938	0.938	0.875	0.913	0.913	0.913
	Median TPR	0.565	0.551	0.471	0.646	0.625	0.583	0.875	0.875	0.750	0.565	0.551	0.471
	Median TNR	0.913	0.913	0.906	0.938	0.896	0.896	0.938	0.938	0.875	0.913	0.913	0.906
Comparison of median of TPR's derived from each observer and reading	(FOV_{40})	1.000	>0.050	>0.050	1.000	>0.050	>0.050	1.000	>0.05	>0.05	1	>0.050	>0.050
	(FOV_{60})		1.000	>0.050		1.000	>0.050		1.000	>0.05		1.000	>0.050
	(FOV_{100})			1.000			1.000			1.000			1.000
Comparison of median of TNR's derived from each observer and reading	(FOV_{40})	1.000	>0.050	>0.050	1.000	>0.050	>0.050	1.000	>0.050	>0.050	1.000	>0.050	>0.050
	(FOV_{60})		1.000	>0.050		1.000	>0.050		1.000	>0.050		1.000	>0.050
	(FOV_{100})			1.000			1.000			1.000			1.000

FOV_{40}, 40 × 40 mm field of view; FOV_{60}, 60 × 60 mm field of view; FOV_{100}, 100 × 100 mm field of view; TPR, true-positive rate; TNR, true-negative rate.

demonstrated.[28] The concordance of our CBCT measurements with actual dimensions validates the use of this methodological approach. However, in applying our results to clinical situations, it should be made clear that it is more difficult to segment unclear buccal peri-implant defects. Indeed, as reported by Agbaje et al,[28] volumes calculated using this approach on CBCT images are smaller than the actual volumes. This is invariably due to inherent difficulties in segmenting the borders of such small defects accurately on CBCT images. Marginal defect calculations on CBCT images have also been performed by Shiratori et al,[29] and compared with measurements from plaster casts. Similar to our study, beam hardening or scatter artefact did not have a significant negative influence on accuracy.

Table 5 Comparison of actual mean depth, width and volume dimensions with cone beam CT measurements

Actual measurements	*Field of view*	n	*Mean*	*Standard deviation*
Actual depth		69	2.97	1.41
Depth (mm)	FOV_{40}	41	3.38	1.31
	FOV_{60}	39	3.44	1.40
	FOV_{100}	33	3.50	1.39
Actual width		69	2.56	1.07
Width (mm)	FOV_{40}	41	2.57	1.02
	FOV_{60}	39	2.64	0.99
	FOV_{100}	33	2.61	0.91
Actual volume		42	24.59	11.73
Volume (mm^3)	FOV_{40}	42	21.42	10.55
	FOV_{60}	42	21.60	10.69
	FOV_{100}	42	21.06	10.66

FOV_{40}, 40 × 40 mm field of view; FOV_{60}, 60 × 60 mm field of view; FOV_{100}, 100 × 100 mm field of view.

Recent guidelines published by the American Academy of Oral and Maxillofacial Radiology[30] recommend cross-sectional imaging be used for the assessment of all dental implant sites and that CBCT is the imaging method of choice for gaining this information. However, in the absence of clinical signs or symptoms, only intraoral periapical radiography is advised for the postoperative assessment of implants. Cross-sectional imaging (particularly CBCT) is advised only immediately post operatively if implant mobility or altered sensation is reported.[30] This recommendation is based on evidence that generally CBCT delivers far greater effective doses than does intraoral imaging. The reported effective dose for the CBCT unit used in this study is in the range of 43–50 μSv.[31] This is higher than the effective doses from periapical radiography taken with E-speed film with rectangular (1–3 μSv) round collimation (1–5 μSv).[32]

A common treatment for peri-implant alveolar defects is the use of guided bone regeneration techniques using synthetic membranes. We found that the CBCT unit used in our study can be useful in determining the presence and dimensions of buccal marginal alveolar defect when a peri-implant defect is suspected. We believe that the CBCT systems that offer restricted FOVs, resolutions <0.3 mm^3 and voxel size low doses may be considered a safe and effective imaging modality preferable to intraoral radiography for use in the assessment of buccal marginal peri-implant defect status in cases where adequate information cannot be obtained by

clinical information alone, especially in cases where one to three implants are to be assessed.

Conclusion

All CBCT images obtained at different FOVs with voxel resolutions <0.3 mm performed similarly in the detection of simulated buccal marginal alveolar peri-implant defects. In addition, depth, width and volume measurements of the defects from CBCT images correlated highly with actual physical measurements. The results of this study are to be considered specific to the one CBCT system evaluated and to situations where streak and beam-hardening artefacts from heavy restoration of the adjacent teeth as well as anatomic noise from the contralateral and opposing jaw structures do not obscure the information sought.

References

1. Jones AA, Cochran DL. Consequences of implant design. *Dent Clin North Am* 2006; **50**: 339–60. doi: 10.1016/j.cden.2006.03.008
2. Mombelli A, Lang NP. Clinical parameters for the evaluation of dental implants. *Periodontol 2000* 1994; **4**: 81–6.
3. Winkler S, Morris HF, Spray JR. Stability of implants and natural teeth as determined by the Periotest over 60 months of function. *J Oral Implantol* 2001; **27**: 198–203. doi: 10.1563/1548-1336(2001)027<0198:SOIANT>2.3.CO;2
4. King GN, Hermann JS, Schoolfield JD, Buser D, Cochran DL. Influence of the size of the microgap on crestal bone levels in non-submerged dental implants: a radiographic study in the canine mandible. *J Periodontol* 2002; **73**: 1111–17. doi: 10.1902/jop.2002.73.10.1111
5. Chung WE, Rubenstein JE, Phillips KM, Raigrodski AJ. Outcomes assessment of patients treated with osseointegrated dental implants at the university of Washington Graduate Prosthodontic Program, 1998 to 2000. *Int J Oral Maxillofac Implants* 2009; **24**: 927–35.
6. Smith DE, Zarb GA. Criteria for success of osseointegrated endosseous implants. *J Prosthet Dent* 1989; **62**: 567–72.
7. Kamburoğlu K, Gulsahi A, Genç Y, Paksoy CS. A comparison of peripheral marginal bone loss at dental implants measured with conventional intraoral film and digitized radiographs. *J Oral Implantol* 2012; **38**: 211–19. doi: 10.1563/AAID-JOI-D-09-00147
8. Schliephake H, Wichmann M, Donnerstag F, Vogt S. Imaging of periimplant bone levels of implants with buccal bone defects. *Clin Oral Implants Res* 2003; **14**: 193–200.
9. Laurell L, Lundgren D. Marginal bone level changes at dental implants after 5 years in function: a meta-analysis. *Clin Implant Dent Relat Res* 2011; **13**: 19–28. doi: 10.1111/j.1708-8208.2009.00182.x
10. Bittar-Cortez JA, Passeri LA, de Almeida SM, Haiter-Neto F. Comparison of peri-implant bone level assessment in digitized conventional radiographs and digital subtraction images. *Dentomaxillofac Radiol* 2006; **35**: 258–62. doi: 10.1259/dmfr/84778143
11. Finne K, Rompen E, Toljanic J. Clinical evaluation of a prospective multicenter study on 1-piece implants. part 1: marginal bone level evaluation after 1 year of follow-up. *Int J Oral Maxillofac Implants* 2007; **22**: 226–34.
12. Piao CM, Lee JE, Koak JY, Kim SK, Rhyu IC, Han CH, et al. Marginal bone loss around three different implant systems: radiographic evaluation after 1 year. *J Oral Rehabil* 2009; **36**: 748–54. doi: 10.1111/j.1365-2842.2009.01988.x
13. Cochran DL, Nummikoski PV, Schoolfield JD, Jones AA, Oates TW. A prospective multicenter 5-year radiographic evaluation of crestal bone levels over time in 596 dental implants placed in 192 patients. *J Periodontol* 2009; **80**: 725–33. doi: 10.1902/jop.2009.080401
14. Gröndahl K, Sundén S, Gröndahl HG. Inter- and intraobserver variability in radiographic bone level assessment at Brånemark fixtures. *Clin Oral Implants Res* 1998; **9**: 243–50.
15. Angelopoulos C, Scarfe WC, Farman AG. A comparison of maxillofacial CBCT and medical CT. *Atlas Oral Maxillofac Surg Clin North Am* 2012; **20**: 1–17. doi: 10.1016/j.cxom.2011.12.008
16. Mengel R, Kruse B, Flores-de-Jacoby L. Digital volume tomography in the diagnosis of peri-implant defects: an *in vitro* study on native pig mandibles. *J Periodontol* 2006; **77**: 1234–41. doi: 10.1902/jop.2006.050424
17. Corpas Ldos S, Jacobs R, Quirynen M, Huang Y, Naert I, Duyck J. Peri-implant bone tissue assessment by comparing the outcome of intra-oral radiograph and cone beam computed tomography analyses to the histological standard. *Clin Oral Implants Res* 2011; **22**: 492–9. doi: 10.1111/j.1600-0501.2010.02029.x
18. Sirin Y, Horasan S, Yaman D, Basegmez C, Tanyel C, Aral A, et al. Detection of crestal radiolucencies around dental implants: an *in vitro* experimental study. *J Oral Maxillofac Surg* 2012; **70**: 1540–50. doi: 10.1016/j.joms.2012.02.024
19. Kamburoğlu K, Kolsuz E, Murat S, Eren H, Yüksel S, Paksoy CS. Assessment of buccal marginal alveolar peri-implant and periodontal defects using a cone beam CT system with and without the application of metal artifact reduction mode. *Dentomaxillofac Radiol* 2013; **42**: 20130176. doi: 10.1259/dmfr.20130176
20. Schulze R, Heil U, Gross D, Bruellmann DD, Dranischnikow E, Schwanecke U, et al. Artefacts in CBCT: a review. *Dentomaxillofac Radiol* 2011; **40**: 265–73. doi: 10.1259/dmfr/30642039
21. Draenert FG, Coppenrath E, Herzog P, Müller S, Mueller-Lisse UG. Beam hardening artefacts occur in dental implant scans with the NewTom cone beam CT but not with the dental 4-row multidetector CT. *Dentomaxillofac Radiol* 2007; **36**: 198–203. doi: 10.1259/dmfr/32579161
22. Esmaeili F, Johari M, Haddadi P, Vatankhah M. Beam hardening artifacts: comparison between two cone beam computed tomography scanners. *J Dent Res Dent Clin Dent Prospects* 2012; **6**: 49–53. doi: 10.5681/joddd.2012.011
23. Cremonini CC, Dumas M, Pannuti CM, Neto JB, Cavalcanti MG, Lima LA. Assessment of linear measurements of bone for implant sites in the presence of metallic artefacts using cone beam computed tomography and multislice computed tomography. *Int J Oral Maxillofac Surg* 2011; **40**: 845–50. doi: 10.1016/j.ijom.2011.04.015
24. Benic GI, Sancho-Puchades M, Jung RE, Deyhle H, Hämmerle CH. *In vitro* assessment of artifacts induced by titanium dental implants in cone beam computed tomography. *Clin Oral Implants Res* 2013; **24**: 378–83. doi: 10.1111/clr.12048
25. Benavides E, Rios HF, Ganz SD, An CH, Resnik R, Reardon GT, et al. Use of cone beam computed tomography in implant dentistry: the international congress of oral implantologists consensus report. *Implant Dent* 2012; **21**: 78–86. doi: 10.1097/ID.0b013e31824885b5
26. Spin-Neto R, Gotfredsen E, Wenzel A. Impact of voxel size variation on CBCT-based diagnostic outcome in dentistry: a systematic review. *J Digit Imaging* 2013; **26**: 813–20. doi: 10.1007/s10278-012-9562-7
27. Razavi T, Palmer RM, Davies J, Wilson R, Palmer PJ. Accuracy of measuring the cortical bone thickness adjacent to dental implants using cone beam computed tomography. *Clin Oral Implants Res* 2010; **21**: 718–25. doi: 10.1111/j.1600-0501.2009.01905.x
28. Agbaje JO, Jacobs R, Maes F, Michiels K, van Steenberghe D. Volumetric analysis of extraction sockets using cone beam computed tomography: a pilot study on *ex vivo* jaw bone. *J Clin Periodontol* 2007; **34**: 985–90. doi: 10.1111/j.1600-051X.2007.01134.x
29. Shiratori LN, Marotti J, Yamanouchi J, Chilvarquer I, Contin I, Tortamano-Neto P. Measurement of buccal bone volume of dental

implants by means of cone-beam computed tomography. *Clin Oral Implants Res* 2012; **23**: 797–804. doi: 10.1111/j.1600-0501.2011.02207.x

30. Tyndall DA, Price JB, Tetradis S, Ganz SD, Hildebolt C, Scarfe WC. Position statement of the American Academy of Oral and Maxillofacial Radiology on selection criteria for the use of radiology in dental implantology with emphasis on cone beam computed tomography. *Oral Surg Oral Med Oral Pathol Oral Radiol* 2012; **113**: 817–26. doi: 10.1016/j.oooo.2012.03.005
31. Pauwels R, Beinsberger J, Collaert B, Theodorakou C, Rogers J, Walker A, et al; SEDENTEXCT Project Consortium. Effective dose range for dental cone beam computed tomography scanners. *Eur J Radiol* 2012; **81**: 267–71. doi: 10.1016/j.ejrad.2010.11.028
32. Gijbels F, Jacobs R, Sanderink G, De Smet E, Nowak B, Van Dam J, et al. A comparison of the effective dose from scanography with periapical radiography. *Dentomaxillofac Radiol* 2002; **31**: 159–63. doi: 10.1038/sj/dmfr/4600683